Electronic Supporting Information (ESI) for

Functionalization of Large-Pore Periodic Mesoporous Silicas: Metal Silylamide and Isopropoxide Molecular Grafting and Secondary Surface Ligand Exchange

Yucang Liang,*[a] Egil Sev. Erichsen[b] and Reiner Anwander*[a]

[a] Anorganische Chemie, Eberhard Karls Universität Tübingen, Auf der Morgenstelle 18, 72076 Tübingen, Germany
[b] Mr. Egil Sev. Erichsen, Laboratory for Electron Microscopy, University of Bergen, Allégaten 41, 5007 Bergen, Norway

* Corresponding author E-mail: yucang.liang@uni-tuebingen.de
reiner.anwander@uni-tuebingen.de

Table S1 Characteristic vibrations of Zn-grafted hybrid SBA-15 materials

Sample	Wavenumber/cm^{-1}								
	O-H	Si-O-Si	C-H	N-H	Si-H	Si-C	Si-N	C-C	C=O	C-N
1	3747	1000~1200, 810, ~670-400	-	-	-	-	-	-	-	-
1a	-	1000~1200, 810, ~670-400	2966, 2908	-	2151, 908	835, 773	-	-	-	-
1b$_{\text{-Zn}}$	-	1000~1200, 810, ~670-400	2953, 2898	-	-	835, 752	884	-	-	-
1c$_{\text{-Zn}}$	-	1000~1200, 808, 670-400	2958, 2897, 1648, 1616	3360, 3025	-	835, 756	-	1498, 915	-	-
1d$_{\text{-Zn}}$	-	1000~1200, 810, ~670-400	2960, 2902, 866	-	-	845, 824, 748	-	1503, 1436	1673, 1652, 1615, 1573, 1386	866
1e$_{\text{-Zn}}$[a]	3603	1000~1200, 810, ~670-400	2960, 2904	-	-	845, 753	-	1498	1698, 1576, 1375	-

Note: SBA-15(**1**);
$HN(SiHMe_2)_2$@SBA-15 (**1a**);
$Zn[N(SiMe_3)_2]_2$@SBA-15 (**1b**$_{\text{-Zn}}$);
$[HO(C_6H_4)OH]$@$Zn[N(SiMe_3)_2]_2$@SBA-15 (**1c**$_{\text{-Zn}}$);
$[HO_2C(C_6H_4)CO_2H]$@$Zn[N(SiMe_3)_2]_2$@SBA-15 (**1d**$_{\text{-Zn}}$);
[a] Data came from the activated material at 120 °C.

Table S2 Characteristic vibrations of Co-grafted hybrid KIT-6 materials

Sample	Wavenumber/cm^{-1}								
	O-H	Si-O-Si	C-H	N-H	Si-H	Si-C	Si-N	C-C	C=O	C-N
2	3747	1000~1200, 810, ~670-400	-	-	-	-	-	-	-	-
2a	-	1000~1200, 810, ~670-400	2966, 2908	-	2151, 908	835, 773	-	-	-	-
2b$_{\text{-Co}}$	-	1000~1200, 810, ~670-400	2952, 2898	-	-	833, 752	878	-	-	-
2c$_{\text{-Co}}$	-	1000~1200, 808, 670-400	2959, 2893, 1652, 1616	3350, 3024	-	826	-	1498, 913	-	-
2d$_{\text{-Co}}$	-	1000~1200, 810, ~670-400	2961, 2905, 866	3318, 3155	-	845, 824, 748	-	1600, 1505, 1436	1670, 1652, 1608, 1393, 1380	866
2d$_{\text{-Co-bp}}$	-	1000~1200, 810, ~670-400	2962, 2903	-	-	847, 765	-	1606, 1519, 1498	1653, 1573, 1409, 1375	-

Note: KIT-6 (**2**);
$HN(SiHMe_2)_2$@KIT-6 (**2a**);
$Co[N(SiMe_3)_2]_2(THF)$@KIT-6 (**2b**$_{\text{-Co}}$);
$[HO(C_6H_4)OH]$@$Co[N(SiMe_3)_2]_2(THF)$@KIT-6 (**2c**$_{\text{-Co}}$);
$[HO_2C(C_6H_4)CO_2H]$@$Co[N(SiMe_3)_2]_2(THF)$@KIT-6 (**2d**$_{\text{-Co}}$);
$[HO_2C(C_6H_4)_2\text{-}CO_2H]$@$Co[N(SiMe_3)_2]_2(THF)$@KIT-6 (**2d**$_{\text{-Co-bp}}$).

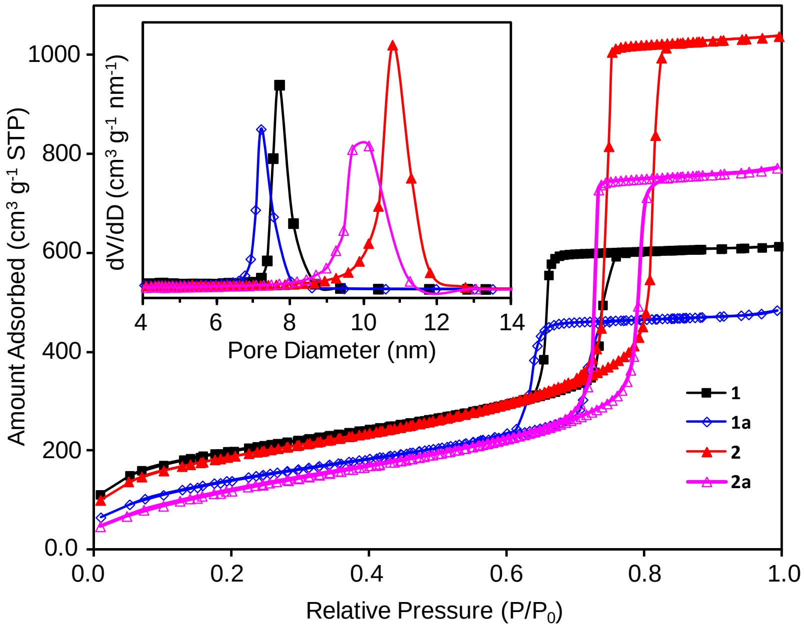

Fig. S1 Nitrogen adsorption-desorption isotherms of parent materials SBA-15 (**1**), KIT-6 (**2**), TMDS-silylated $HN(SiHMe_2)_2$@SBA-15 (**1a**) and $HN(SiHMe_2)_2$@KIT-6 (**2a**). The inset shows the BJH pore size distribution calculated from the adsorption branch of isotherm.

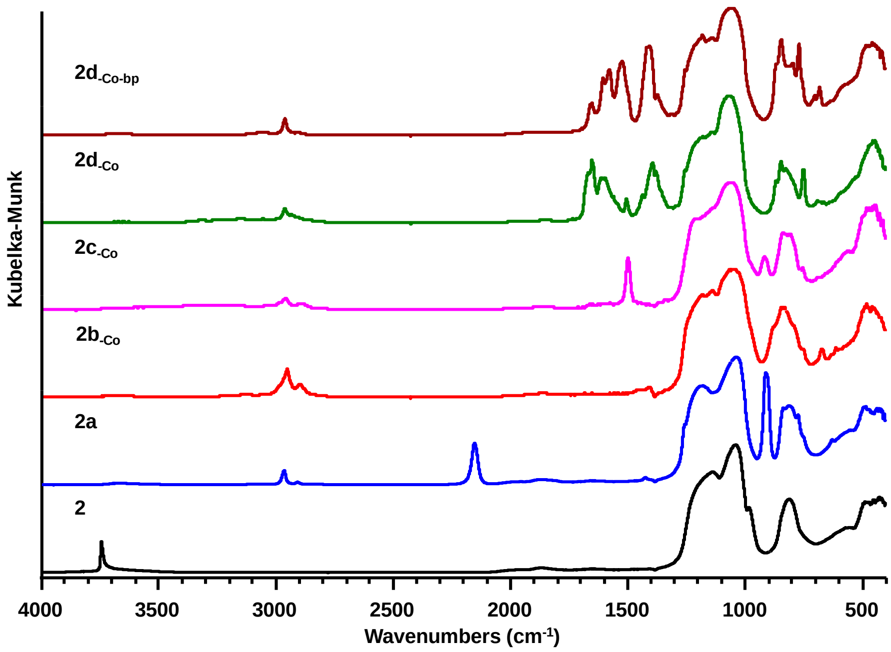

Fig. S2 DRIFT spectra of parent material KIT-6 (**2**), TMDS-silylated $HN(SiHMe_2)_2$@KIT-6 (**2a**), $Co[N(SiMe_3)_2]_2(THF)$@KIT-6 (**2b**$_{\text{-Co}}$), $[HO(C_6H_4)OH]$@$Co[N(SiMe_3)_2]_2(THF)$@KIT-6 (**2c**$_{\text{-Co}}$), $[HO_2C(C_6H_4)CO_2H]$@$Co[N(SiMe_3)_2]_2(THF)$@KIT-6 (**2d**$_{\text{-Co}}$) and $[HO_2C(C_6H_4)_2$-$CO_2H]$@$Co[N(SiMe_3)_2]_2(THF)$@KIT-6 (**2d**$_{\text{-Co-bp}}$).

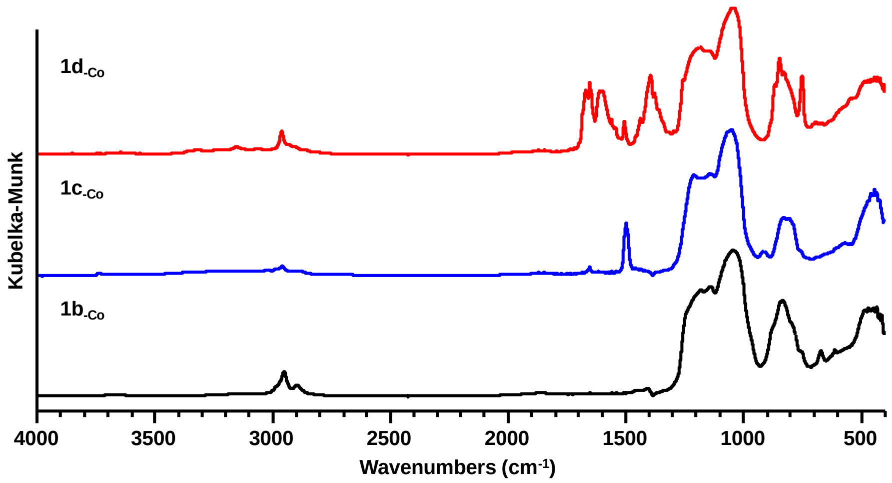

Fig. S3 DRIFT spectra of the Co-modified hexagonal Co[N(SiMe$_3$)$_2$]$_2$(THF)@SBA-15 (**1b$_{\text{-Co}}$**), [HO(C$_6$H$_4$)OH]@Co[N(SiMe$_3$)$_2$]$_2$(THF)@SBA-15 (**1c$_{\text{-Co}}$**) and [HO$_2$C(C$_6$H$_4$)CO$_2$H]@-Co[N(SiMe$_3$)$_2$]$_2$(THF)@SBA-15 (**1d$_{\text{-Co}}$**).

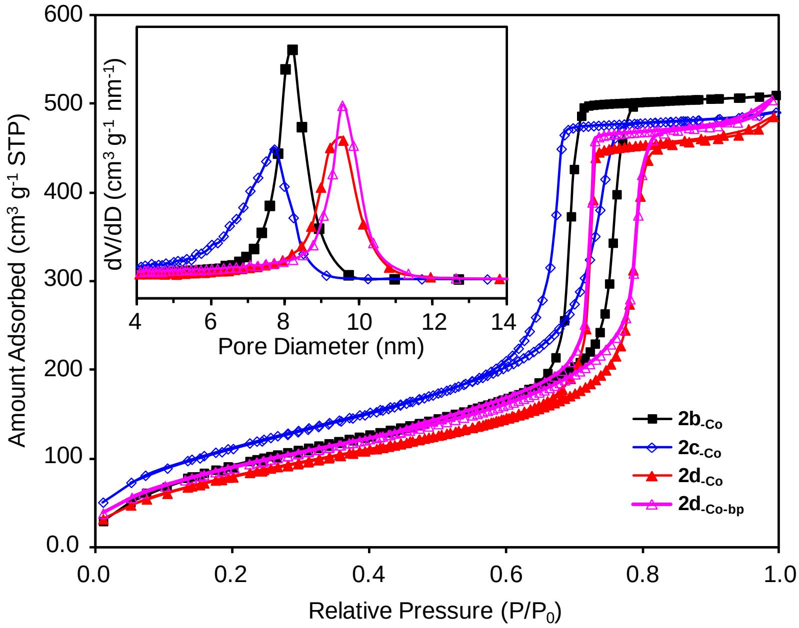

Fig. S4 Nitrogen adsorption-desorption isotherms of Co[N(SiMe$_3$)$_2$]$_2$(THF)@KIT-6 (**2b$_{\text{-Co}}$**), [HO(C$_6$H$_4$)OH]@Co[N(SiMe$_3$)$_2$]$_2$(THF)@KIT-6 (**2c$_{\text{-Co}}$**), [HO$_2$C(C$_6$H$_4$)CO$_2$H]@Co[N(Si-Me$_3$)$_2$]$_2$(THF)@KIT-6 (**2d$_{\text{-Co}}$**) and [HO$_2$C(C$_6$H$_4$)$_2$CO$_2$H]@Co[N(SiMe$_3$)$_2$]$_2$(THF)@KIT-6 (**2d$_{\text{-Co-bp}}$**). The inset shows the BJH pore size distribution calculated from the adsorption branch of isotherm.

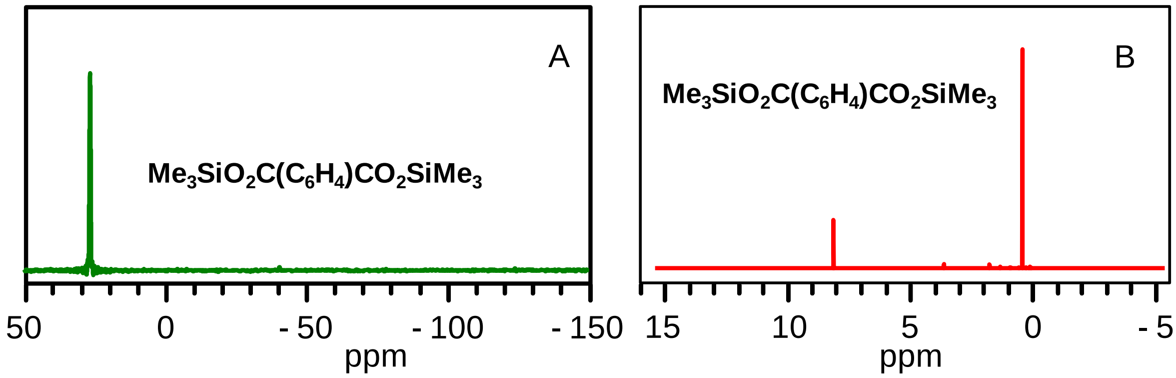

Fig. S5 A) The solid state ^{29}Si CP MAS NMR and B) liquid-phase ^{1}H NMR (THF-d_8) of organic complex $Me_3SiO_2C(C_6H_4)CO_2SiMe_3$.

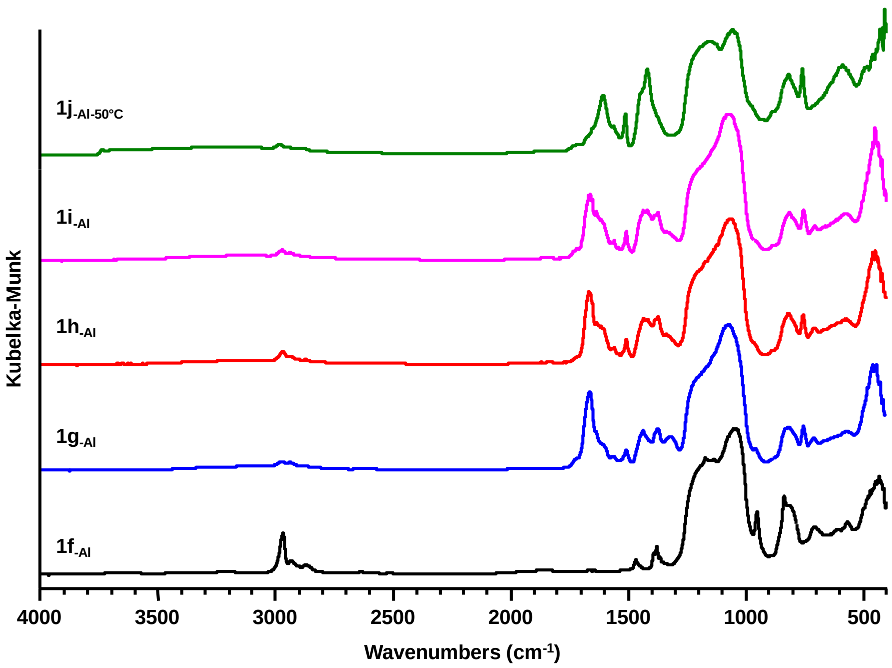

Fig. S6 DRIFT spectra of the Al-hybrid materials $\{Al(OCHMe_2)_3\}$@SBA-15 (**1f**$_{-Al}$), $[HO_2C(C_6H_4)CO_2H]$@$\{Al(OCHMe_2)_3\}$@SBA-15 (**1g**$_{-Al}$), $\{Al(OCHMe_2)_3\}$@$[HO_2C(C_6H_4)$-$CO_2H]$@$\{Al(OCHMe_2)_3\}$@SBA-15 (**1h**$_{-Al}$), $[HO_2C(C_6H_4)CO_2H]$@$\{Al(OCHMe_2)_3\}$@-$[HO_2C(C_6H_4)CO_2H]$@$\{Al(OCHMe_2)_3\}$@SBA-15 (**1i**$_{-Al}$) and $[HO_2C(C_6H_4)CO_2]_yAl(OH)_x$-@SBA-15 (**1j**$_{-Al}$).

Table S3 Characteristic vibrations of Al-grafted hybrid SBA-15 materials

Sample	Wavenumber/cm^{-1}						
	O-H	Si-O-Si	C-H	Al-O	Si-O-Al	C-C	C=O
1	3747	1000~1200, 810, ~670-400	-	-	-	-	-
1f$_{\text{-Al}}$	3706	1000~1200, 810, ~670-400	2968, 2934, 2870	949	835, 704	-	-
1g$_{\text{-Al}}$	-	1000~1200, 816, ~670-400	2972, 2938,2877	962	751, 707	1607, 1507, 1436	1663, 1374,
1h$_{\text{-Al}}$	-	1000~1200, 816, ~670-400	2972, 2938,2877	962	751, 707	1607, 1507, 1436	1663, 1374,
1i$_{\text{-Al}}$	-	1000~1200, 816, ~670-400	2972, 2938,2877	962	751, 707	1607, 1507, 1436	1663, 1374,
1j$_{\text{-Al}}$[a]	3740	1000~1200, 816, ~670-400	2983, 2878	962	751, 707	1602, 1506, 1420	1557

Note: SBA-15 (**1**);
$\{Al(OCHMe_2)_3\}$@SBA-15 (**1f**$_{\text{-Al}}$);
$[HO_2C(C_6H_4)CO_2H]$@$\{Al(OCHMe_2)_3\}$@SBA-15 (**1g**$_{\text{-Al}}$);
$\{Al(OCHMe_2)_3\}$@$[HO_2C(C_6H_4)CO_2H]$@$\{Al(OCHMe_2)_3\}$@SBA-15 (**1h**$_{\text{-Al}}$);
$[HO_2C(C_6H_4)CO_2H]$@$\{Al(OCHMe_2)_3\}$@$[HO_2C(C_6H_4)CO_2H]$@$\{Al(OCHMe_2)_3\}$@SBA-15 (**1i**$_{\text{-Al}}$);
$[HO_2C(C_6H_4)CO_2]_yAl(OH)_x$@SBA-15 (**1j**$_{\text{-Al}}$).
[a] Data came from the activated material at 50 °C.

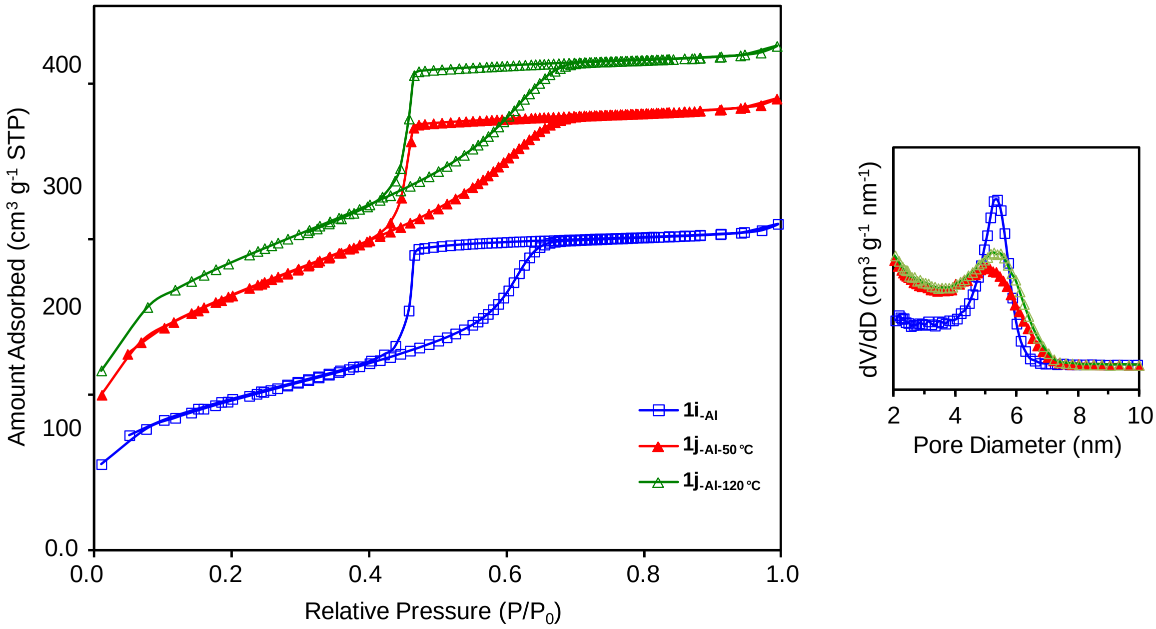

Fig. S7 Nitrogen adsorption-desorption isotherms (left) and the BJH pore size distribution (right) calculated from the adsorption branch of isotherm for materials $[HO_2C(C_6H_4)CO_2H]$-@$\{Al(OCHMe_2)_3\}$@$[HO_2C(C_6H_4)CO_2H]$@$\{Al(OCHMe_2)_3\}$@SBA-15 (**1i**$_{\text{-Al}}$) and $[HO_2C(C_6H_4)CO_2]_yAl(OH)_x$@SBA-15 (**1j**$_{\text{-Al}}$, dried at 50 °C and 120 °C).

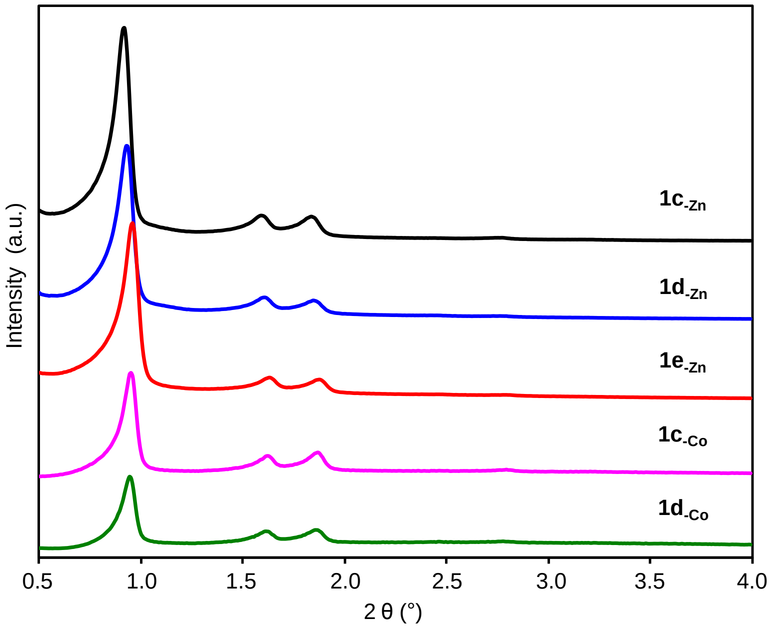

Fig. S8 Low-angle PXRD patterns of hybrid materials [HO(C_6H_4)OH]@Zn[N(Si-Me_3)$_2$]$_2$@SBA-15 (**1c**$_{\mathbf{-Zn}}$), [HO_2C(C_6H_4)CO_2H]@Zn[N($SiMe_3$)$_2$]$_2$@SBA-15 (**1d**$_{\mathbf{-Zn}}$), [HO_2C-(C_6H_4)CO_2]Zn(DMF)$_y$(H_2O)$_x$@SBA-15 (**1e**$_{\mathbf{-Zn}}$), [HO(C_6H_4)OH]@Co[N($SiMe_3$)$_2$]$_2$(THF)@-SBA-15 (**1c**$_{\mathbf{-Co}}$) and [HO_2C(C_6H_4)CO_2H]@Co[N($SiMe_3$)$_2$]$_2$(THF)@SBA-15 (**1d**$_{\mathbf{-Co}}$).

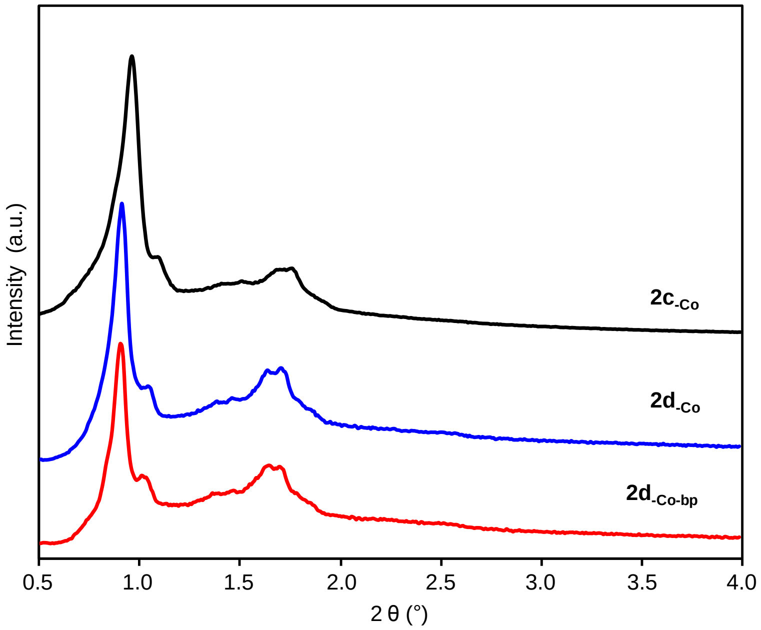

Fig. S9 Low-angle PXRD patterns of hybrid materials [HO(C_6H_4)OH]@Co[N($SiMe_3$)$_2$]$_2$-(THF)@KIT-6 (**2c**$_{\mathbf{-Co}}$), [HO_2C(C_6H_4)CO_2H]@Co[N($SiMe_3$)$_2$]$_2$(THF)@KIT-6 (**2d**$_{\mathbf{-Co}}$) and [HO_2C(C_6H_4)$_2$$CO_2H$]@Co[N($SiMe_3$)$_2$]$_2$(THF)@KIT-6 (**2d**$_{\mathbf{-Co-bp}}$).

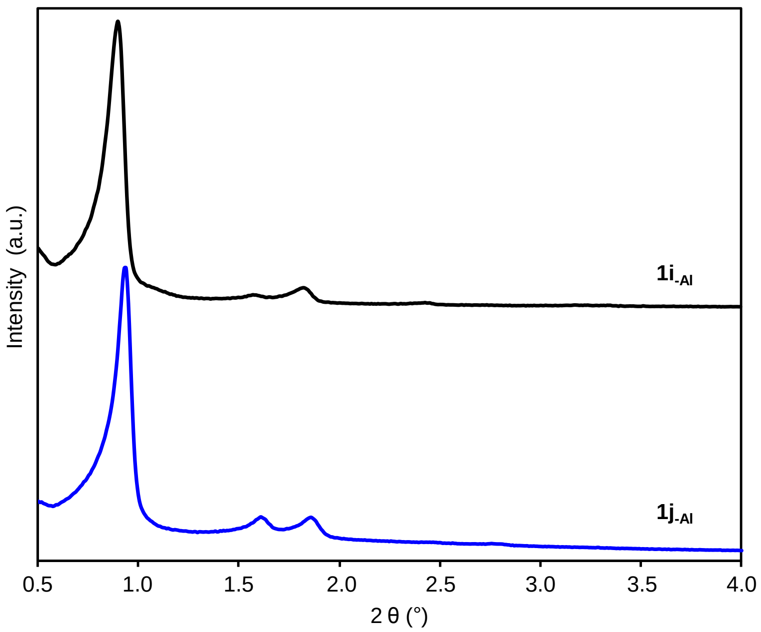

Fig. S10 Low-angle PXRD patterns of hybrid materials $[HO_2C(C_6H_4)CO_2H]$@-$\{Al(OCHMe_2)_3\}$@$[HO_2C(C_6H_4)CO_2H]$@$\{Al(OCHMe_2)_3\}$@SBA-15 (**1i**$_{\text{-}\mathbf{Al}}$) and $[HO_2C(C_6H_4)CO_2]_yAl(OH)_x$@SBA-15 (**1j**$_{\text{-}\mathbf{Al}}$).

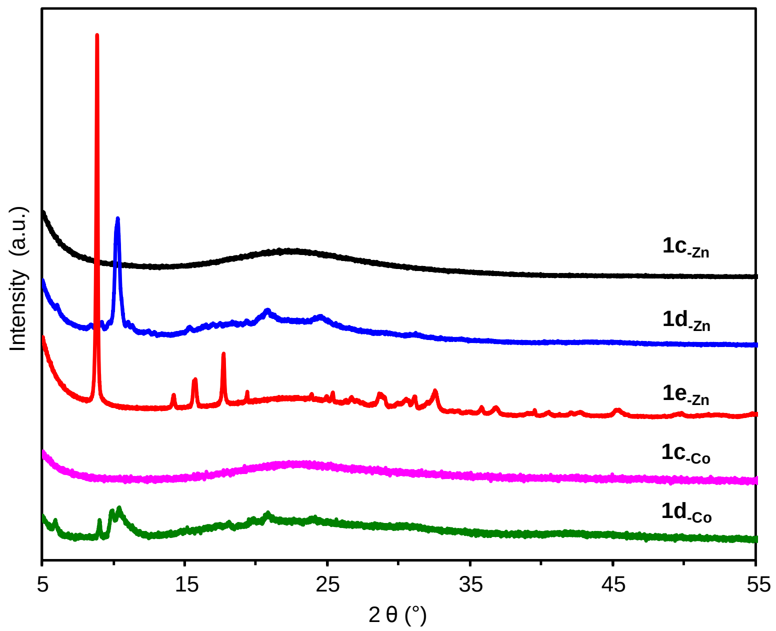

Fig. S11 Wide-angle PXRD patterns of hybrid materials $[HO(C_6H_4)OH]$@$Zn[N(SiMe_3)_2]_2$-@SBA-15 (**1c**$_{\text{-}\mathbf{Zn}}$), $[HO_2C(C_6H_4)CO_2H]$@$Zn[N(SiMe_3)_2]_2$@SBA-15 (**1d**$_{\text{-}\mathbf{Zn}}$), $[HO_2C(C_6H_4)$-$CO_2]Zn(DMF)_y(H_2O)_x$@SBA-15 (**1e**$_{\text{-}\mathbf{Zn}}$), $[HO(C_6H_4)OH]$@$Co[N(SiMe_3)_2]_2(THF)$@SBA-15 (**1c**$_{\text{-}\mathbf{Co}}$) and $[HO_2C(C_6H_4)CO_2H]$@$Co[N(SiMe_3)_2]_2(THF)$@SBA-15 (**1d**$_{\text{-}\mathbf{Co}}$).

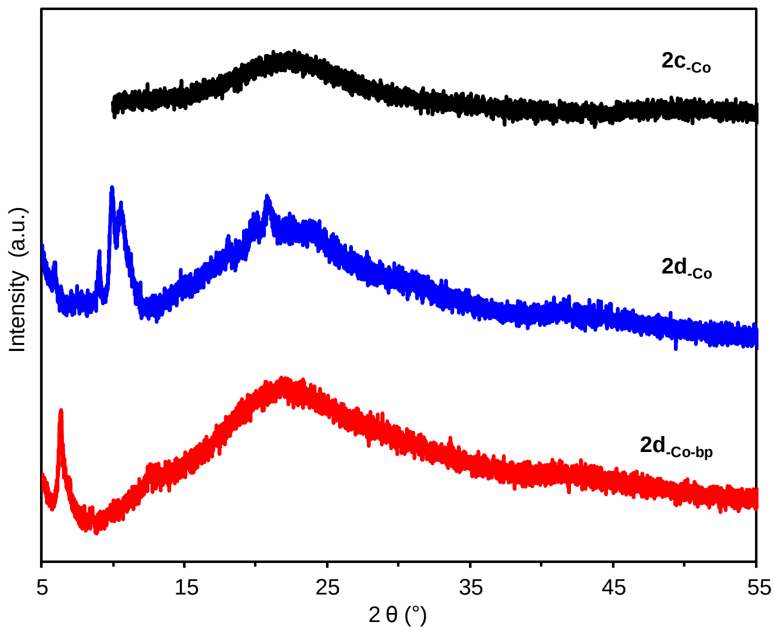

Fig. S12 Wide-angle PXRD patterns of hybrid materials $[HO(C_6H_4)OH]@Co[N(SiMe_3)_2]_2$-(THF)@KIT-6 (**2c**$_{\textbf{-Co}}$), $[HO_2C(C_6H_4)CO_2H]@Co[N(SiMe_3)_2]_2$(THF)@KIT-6 (**2d**$_{\textbf{-Co}}$) and $[HO_2C(C_6H_4)_2CO_2H]@Co[N(SiMe_3)_2]_2$(THF)@KIT-6 (**2d**$_{\textbf{-Co-bp}}$).

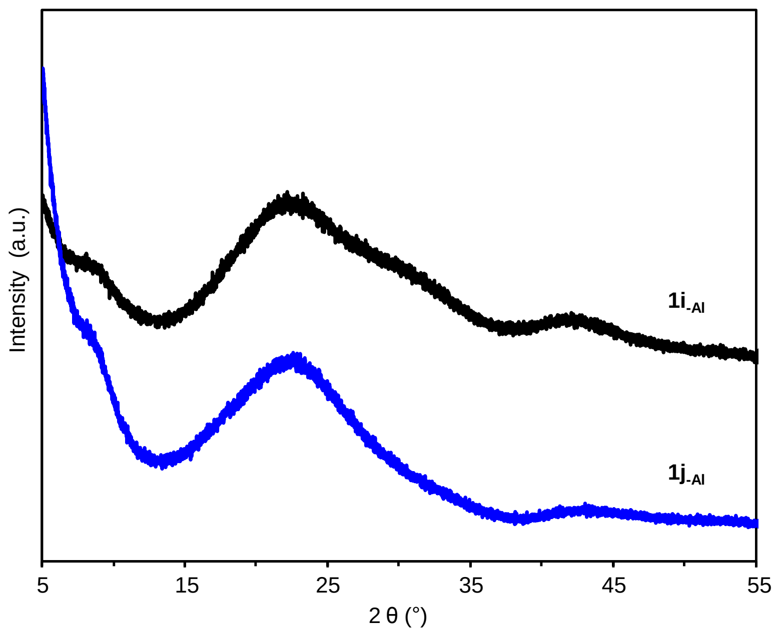

Fig. S13 wide-angle PXRD patterns of hybrid materials $[HO_2C(C_6H_4)CO_2H]$@-$\{Al(OCHMe_2)_3\}@[HO_2C(C_6H_4)CO_2H]@\{Al(OCHMe_2)_3\}$@SBA-15 (**1i**$_{\textbf{-Al}}$) and $[HO_2C$-$(C_6H_4)CO_2]_yAl(OH)_x$@SBA-15 (**1j**$_{\textbf{-Al}}$).

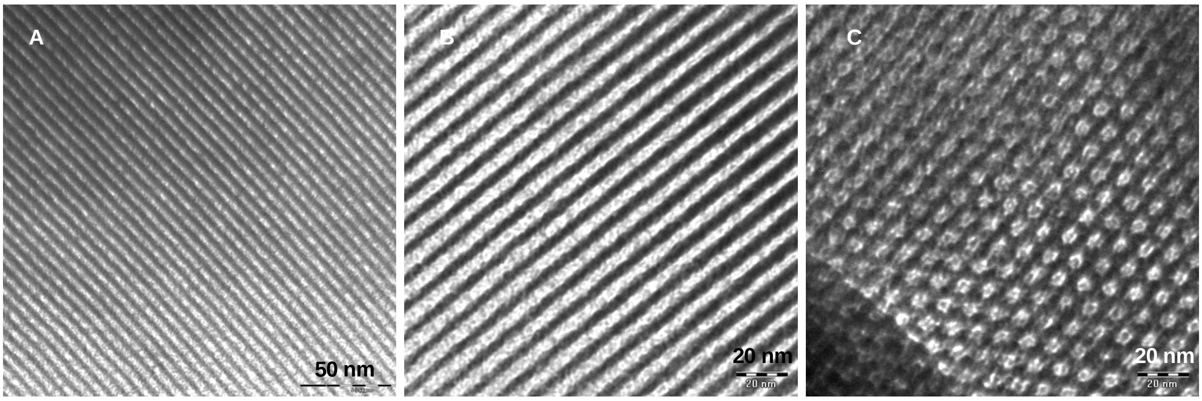

Fig. S14 The representative TEM images taken along the direction perpendicular to the pore axis (A) for hybrid material $[HO(C_6H_4)OH]@Co[N(SiMe_3)_2]_2(THF)@SBA\text{-}15$ (**1c**$_{\textbf{-Co}}$), (B) for hybrid material $[HO_2C(C_6H_4)CO_2H]@Co[N(SiMe_3)_2]_2(THF)@SBA\text{-}15$ (**1d**$_{\textbf{-Co}}$) and the direction of the pore axis (C) for material **1d**$_{\textbf{-Co}}$.

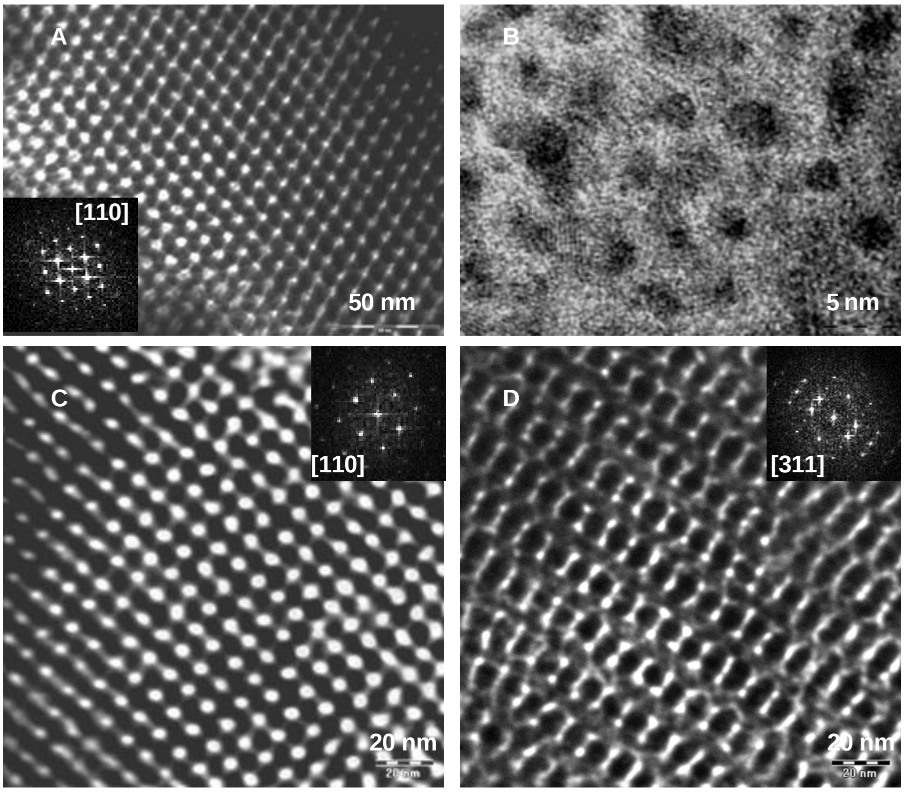

Fig. S15 The representative TEM images taken along [110] direction (A) and high-resolution TEM image (B) for hybrid material $[HO(C_6H_4)OH]@Co[N(SiMe_3)_2]_2(THF)@KIT\text{-}6$ (**2c**$_{\textbf{-Co}}$), [110] (C) and [311] (D) for hybrid material $[HO_2C(C_6H_4)CO_2H]@Co[N(SiMe_3)_2]_2$-$(THF)@KIT\text{-}6$ (**2d**$_{\textbf{-Co}}$).

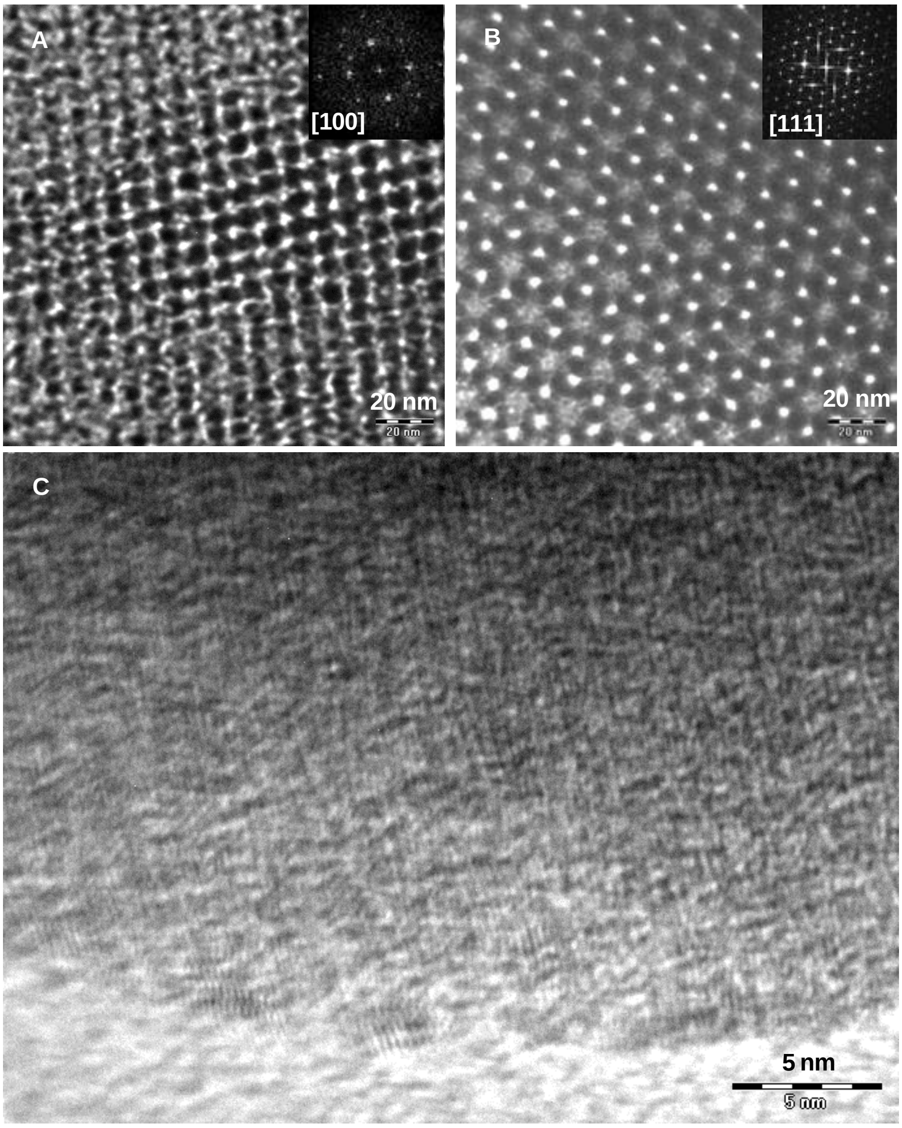

Fig. S16 The representative TEM images taken along [100] (A), [111] (B) direction and high-resolution TEM image (C) for hybrid material $[HO_2C(C_6H_4)_2CO_2H]@Co[N(SiMe_3)_2]_2$-(THF)@KIT-6 (**2d**$_{\text{-Co-bp}}$).

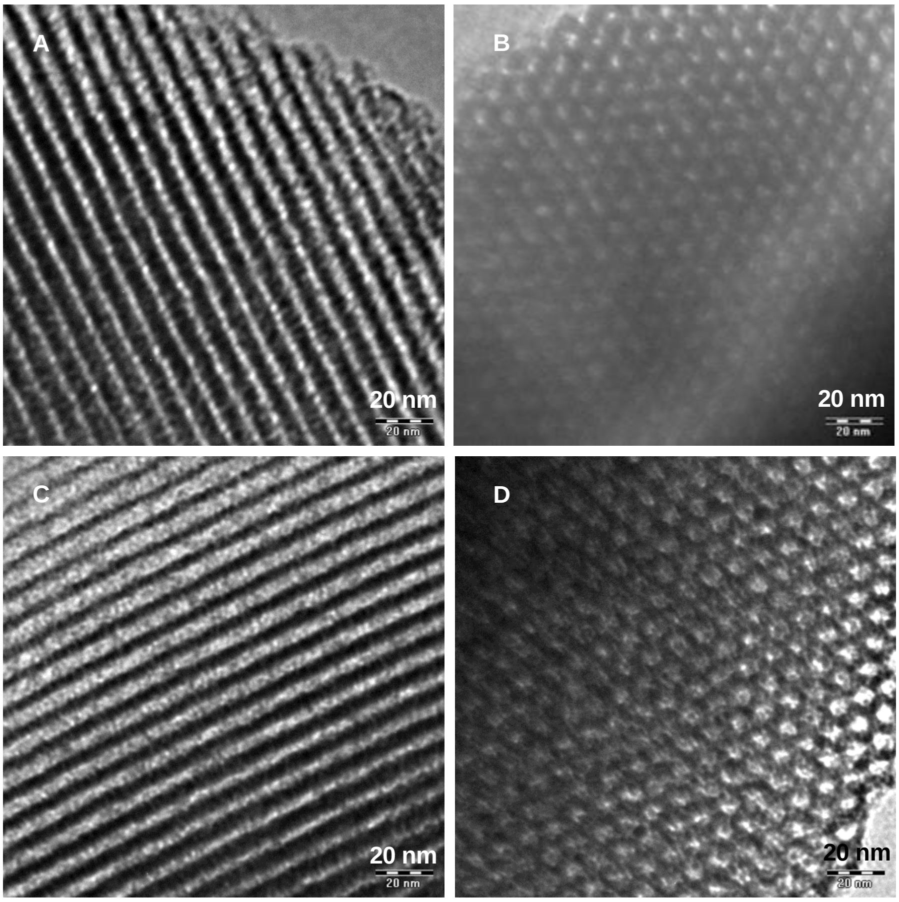

Fig. S17 The representative TEM images taken along the direction perpendicular to the pore axis (A) and the pore axis (B) for hybrid materials $[HO_2C(C_6H_4)CO_2H]$@-$\{Al(OCHMe_2)_3\}$@$[HO_2C(C_6H_4)CO_2H]$@$\{Al(OCHMe_2)_3\}$@SBA-15 (**1i$_{-Al}$**), and direction perpendicular to the pore axis (C) and the pore axis (D) for hybrid materials $[HO_2C(C_6H_4)CO_2]_yAl(OH)_x$@SBA-15 (**1j$_{-Al}$**).